9 Lidars and wind turbine control – Part 1

David Schlipf
Stuttgart Chair of Wind Energy, Institute of Aircraft Design, Universität Stuttgart, Germany

9.1 Introduction

In recent years lidar technology found its way into wind energy. The main application is still the site assessment, but the possibility to optimize the energy production and reduce the loads by nacelle or spinner based lidar systems is becoming an important issue. In terms of control the inflowing wind field is the main disturbance to the wind turbine and most of the wind turbine control is designed to deal with variations in this disturbance. From control theory, the control performance can be improved with the knowledge of the disturbance. Due to the measurement principle and the complexity of the wind lidar assisted control is a wide field of research. The main idea is to divide the problem in a measurement and a control problem.

The presented work describes first how wind characteristics, such as wind speed, direction and shears, can be reconstructed from the limited provided information (see Section 9.2). Based on the models of the wind turbines (see Section 9.3) it is investigated in Section 9.4, how well the lidar information can be correlated to the turbines reaction.

In the next sections, several controllers are presented, see Table 15. All controllers are designed first for the case of perfect measurement and then adjusted for realistic measurements. The most promising approach is the collective pitch feedforward controller using the knowledge of the incoming wind speed providing an additional control update to assist common collective pitch control. Additional load reduction compared to the sophisticated feedback controllers could be archived (Schlipf et al., 2010a). The concept has been successfully tested on two research wind turbines (Schlipf et al., 2012a; Scholbrock et al., 2013). Then a feedforward control strategy to increase the energy production by tracking optimal inflow conditions is presented. The comparison to existing indirect speed control strategies shows a marginal increase in energy output at the expense of raised fluctuations of the generator torque (Schlipf et al., 2011). A Nonlinear Model Predictive Control (NMPC) is also presented, which predicts and optimizes the future behavior of a wind turbine using the wind speed preview adjusting simultaneously the pitch angle and the generator torque. The NMPC achieves further load reductions especially for wind conditions near rated wind speed (Schlipf et al., 2012b). Furthermore, a cyclic pitch feedforward controller using the measured horizontal and vertical shear is introduced to assist common cyclic pitch control for further reduction of blade loads. Simulations results from Dunne et al. (2012) are promising, but they have to be further investigated under more realistic conditions. Finally, the benefit of lidar assisted yaw control is explored. A promising way to obtain a accurate measurement of the wind direction is to measure it over the full rotor plane ahead of the turbine by lidar. The expected increase of the energy output is about one percent of the annual energy production, when using the wind direction signal from the lidar system instead of the sonic anemometer (Schlipf et al., 2011).

9.2 Model Based Wind Field Reconstruction

In this section a method is proposed to retrieve the necessary information for lidar assisted control out of lidar data. First the ambiguity in wind field reconstruction is presented. Then lidar and wind models are introduced which can be applied to reconstruct wind characteristics. Further details can be found in Schlipf et al. (2011) and Schlipf et al. (2012c).

Table 15: Possible application and benefit of lidar assisted control.

	benefit	potential	Section
collective pitch feedforward	less loads	$< 20\%$	9.5
direct speed control	more energy	marginal	9.6
model predictive control	more energy + less loads	$< 1\% + < 30\%$	9.7
cyclic pitch feedforward	less loads	$< 20\%$	9.8
lidar assisted yaw control	more energy	$< 2\%$	9.9

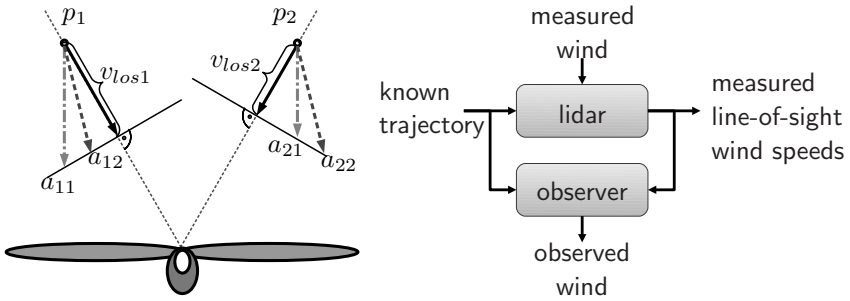

Figure 116: (left) Ambiguity in wind field reconstruction. (right) System theoretical view on lidar measurements and wind field reconstruction.

9.2.1 Ambiguity in Wind Field Reconstruction

It is not possible to measure a three-dimensional wind vector with a single nacelle or spinner based lidar system due to the limitation to the line-of-sight wind speed. But with simple assumptions the wind vector can be reconstructed:

1. no vertical and no horizontal wind component
2. no vertical component and homogeneous flow

In Figure 116 the effect of both assumptions is shown. In this example the 3D vectors in the locations p_1 and p_2 (measured at the same height) are reconstructed from the line-of-sight wind speeds $v_{los,1}$ and $v_{los,2}$. The first assumption yields a_{11} and a_{21} representing a horizontal shear. By the second assumption the resulting vectors a_{12} and a_{22} are equal representing a cross-flow. A dilemma ("Cyclops Dilemma") exists, if the lidar is used for yaw and cyclic pitch control at the same time: If the first assumption is used to calculate the inhomogeneous inflow, perfect alignment is assumed. If the second assumption is used to obtain the misalignment, homogeneous flow is assumed.

9.2.2 Lidar Model for Reconstruction

All known settings of a lidar system can be considered as inputs, all unknown influences as disturbances and the measurements as outputs (see Figure 116). In system theory a disturbance observer can be used to reconstruct the disturbances from the system in- and outputs, if observability is given. Robustness evaluates, how well this is done in the presence of model and measurement uncertainties. For static systems observability and robustness can be simplified to the questions, whether a unique disturbance can be found which caused the measured output with given input and how sensible it is for uncertainties. For this purpose, a model of the system is needed, similar to a simulation model and the observation can be considered to be inverse to a simulation.

A lidar measuring in point i can be modeled by

$$v_{los,i} = \frac{x_i}{f_i}u_i + \frac{y_i}{f_i}v_i + \frac{z_i}{f_i}w_i, \tag{184}$$

which is a projection of the wind vector $[u_i\ v_i\ w_i]$ and the normalized vector of the laser beam focusing in the point $[x_i\ y_i\ z_i]$ with a focus length f_i. Since there is only one equation

for three unknowns, it is impossible to reconstruct the local wind vector. Observability can be restored by changing the wind model, which has to be chosen according to the application and the quality of the results depends on the model validity.

9.2.3 Wind Model for Collective Pitch Control

The simplest model assumes that only the rotor effective wind v_0 is present and no shears or inflow angles. In this case, the u_i component is equal to the rotor effective wind, v_i and w_i are neglected. Using (184) the rotor effective wind estimate v_{0L} can be defined for n points measured in the same vertical measurement plane in front of the turbine as:

$$v_{0L} = \frac{1}{n}\sum_{i}^{n} v_{los,i}\frac{f_i}{x_i}. \tag{185}$$

9.2.4 Wind Model for Cyclic Pitch Control

In the second model, it is assumed that the wind is homogeneous in a vertical measurement plane in front of the turbine. If there is no tilted inflow and no misalignment, the turbulent wind vector field is reduced to v_0 and the horizontal and vertical shear (δ_H and δ_V):

$$u_i = v_0 + \delta_H y_i + \delta_V z_i. \tag{186}$$

The advantage of this reduction is that n measurements gathered simultaneously in the same measurement plane can be combined to get an estimation for the rotor effective wind characteristics. For non simultaneous measurements of scanning systems, the last n focus points of a scan can be used. Following equation is obtained using (186) and (184):

$$\underbrace{\begin{bmatrix} v_{los,1} \\ \vdots \\ v_{los,n} \end{bmatrix}}_{m} = \underbrace{\begin{bmatrix} x/f_1 & xy_1/f_1 & xz_1/f_1 \\ \vdots & \vdots & \vdots \\ x/f_n & xy_n/f_n & xz_n/f_n \end{bmatrix}}_{A} \underbrace{\begin{bmatrix} v_0 \\ \delta_H \\ \delta_V \end{bmatrix}}_{s}. \tag{187}$$

A solution for all three wind characteristics can only be found, if $rank(A) = 3$. For $n = 3$ there is one unique solution

$$s = [v_0 \ \delta_H \ \delta_V]^T = A^{-1}m. \tag{188}$$

For $n > 3$ a solution can be selected by the method of least squares.

9.2.5 Wind Model for Yaw Control

This model assumes that there is no shear and no tilted inflow and that the u and v wind component are homogeneous. Using (184) a linear system in u and v can be formulated:

$$\underbrace{\begin{bmatrix} v_{los,1} \\ \vdots \\ v_{los,n} \end{bmatrix}}_{m} = \underbrace{\begin{bmatrix} x/f_1 & y_1/f_1 \\ \vdots & \vdots \\ x/f_n & y_n/f_n \end{bmatrix}}_{A} \underbrace{\begin{bmatrix} u \\ v \end{bmatrix}}_{s}. \tag{189}$$

This system can be solved using the estimator (188), if $rank(A) = 2$.

9.2.6 Wind Model for Complex Terrain

In the presence of inflow angles and shears the measurement in point i can be defined as

$$u_{Wi} = v_0 + \delta_H y_{Wi} + \delta_V z_{Wi}, \tag{190}$$

The wind coordinates $[x_{Wi} \ y_{Wi} \ z_{Wi}]$ can be transformed to the lidar coordinate system by a rotation of the horizontal and vertical inflow angle, α_H and α_V. A numerical inversion for

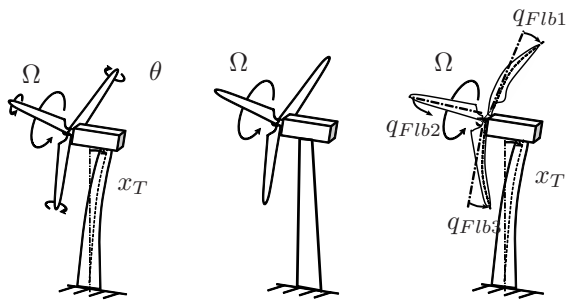

Figure 117: Degrees of freedom for the reduced nonlinear model (left), the first order model (center) and the linear model (right).

the nonlinear equations can be achieved with the least-squares minimization problem

$$\min_{v_0,\alpha_H,\alpha_V,\delta_H,\delta_V} \sum_{i=1}^{n} \left(v_{los,i} - \frac{x_{Wi}}{f_i} u_{Wi} \right)^2, \tag{191}$$

and the wind vector can be calculated with (190) and the inverse transformation.

9.3 Modeling of the Wind Turbine

The crucial part of a successful feedforward and model predictive controller design is the adequate modeling of the dynamic system to be controlled. The model should be simple enough to allow a partial system inversion (for the feedforward controller design) and simulations in reasonable computation time (for the NMPC) and at the same time it should be accurate enough to capture the system dynamics that are relevant for the wind turbine control. The reduced model can also be used in an estimator to estimate the rotor effective wind speed from turbine data.

9.3.1 Reduced Nonlinear Model

Classically aeroelastic simulation environments for wind turbines such as FAST (Jonkman and Buhl, 2005) (used later in this work) provide models close to reality but far to complex to be used for controller design. In addition, current remote sensing methods such as lidar are not able to provide a wind field estimate with comparable details to a generic wind field used by aeroelastic simulations (generated in this work with TurbSim (Jonkman and Buhl, 2007)). In this section a turbine model with three degrees of freedom (see Figure 117) is derived from physical fundamentals and the wind field is reduced to the rotor effective wind speed which is measurable with existing lidar technology.

The first tower fore-aft bending mode, the rotational motion and the collective pitch actuator are based on Bottasso et al. (2006):

$$J\dot{\Omega} + M_g/i = M_a(\dot{x}_T, \Omega, \theta, v_0) \tag{192a}$$

$$m_{Te}\ddot{x}_T + c_T\dot{x}_T + k_T x_T = F_a(\dot{x}_T, \Omega, \theta, v_0) \tag{192b}$$

$$\ddot{\theta} + 2\xi\omega\dot{\theta} + \omega^2(\theta - \theta_c) = 0. \tag{192c}$$

Equation (192a) models the drive-train dynamics, where Ω is the rotor speed, M_a is the aerodynamic torque and M_g the electrical generator torque, x_T the tower top fore-aft displacement, θ the effective collective blade pitch angle, and v_0 the rotor effective wind speed. Moreover, i is the gear box ratio and J is the sum of the moments of inertia about the rotation axis of the rotor hub, blades and the electric generator. Equation (192b) describes the tower fore-aft dynamics, F_a is the aerodynamic thrust and m_{Te}, c_T, and k_T are the tower equivalent modal mass, structural damping and bending stiffness, respectively. These values were calculated according to Jonkman et al. (2009). Finally, equation (192c) is a second-order

model of the blade pitch actuator, where ω is the undamped natural frequency and ξ the damping factor of the pitch actuator and θ_c is the collective blade pitch control input. The nonlinearity in the reduced model resides in the aerodynamic thrust and torque acting on the rotor with the radius R:

$$M_a(\dot{x}_T, \Omega, \theta, v_0) = \frac{1}{2}\rho\pi R^3 \frac{c_P(\lambda,\theta)}{\lambda} v_{rel}^2 \tag{193a}$$

$$F_a(\dot{x}_T, \Omega, \theta, v_0) = \frac{1}{2}\rho\pi R^2 c_T(\lambda,\theta) v_{rel}^2, \tag{193b}$$

where ρ is the air density, λ the tip-speed ratio, defined as

$$\lambda = \frac{\Omega R}{v_{rel}}, \tag{194}$$

and c_P and c_T are the effective power and thrust coefficients, respectively. The nonlinear c_P and c_T coefficients can be obtained from steady state simulation. The relative wind speed v_{rel} is defined as a superposition of tower top speed and mean wind speed

$$v_{rel} = (v_0 - \dot{x}_T), \tag{195}$$

and is used to model the aerodynamic damping. The equations (192) to (195) can be organized in the usual nonlinear state space form:

$$\begin{aligned} \dot{x} &= f(x,u,d) \\ y &= h(x,u,d), \end{aligned} \tag{196}$$

where the states x, the inputs u, disturbance d and measurable outputs y are

$$x = \begin{bmatrix} \Omega & x_T & \dot{x}_T & \theta & \dot{\theta} \end{bmatrix}^T, \qquad u = \begin{bmatrix} M_g & \theta_c \end{bmatrix}^T,$$

$$d = v_0, \qquad y = \begin{bmatrix} \Omega & \ddot{x}_T & \theta & \dot{\theta} \end{bmatrix}^T.$$

9.3.2 Estimation of the Rotor Effective Wind Speed from Turbine Data

The nonlinear reduced model (192) can be further reduced to a first order system (see Figure 117) by ignoring the tower movement and the pitch actuator:

$$J\dot{\Omega} + M_g/i = M_a(\Omega, \theta, v_0) \tag{197a}$$

$$M_a(\Omega, \theta, v_0) = \frac{1}{2}\rho\pi R^3 \frac{c_P(\lambda,\theta)}{\lambda} v_0^2 \tag{197b}$$

$$\lambda = \frac{\Omega R}{v_0}. \tag{197c}$$

This model is used to estimate the rotor effective wind speed v_0 from turbine data. If parameter such as inertia J, gear box ratio i and rotor radius R as well as the power coefficient $c_P(\lambda,\theta)$ are known, and data such as generator torque M_g, pitch angle θ, rotor speed Ω and air density ρ are measurable, the only unknown in (197) is the rotor effective wind v_0.

Due to the λ-dependency of the power coefficient $c_P(\lambda,\theta)$ no explicit solution can be found. A solution could be found by solving (197) by iterations. But this would produce high computational effort for high resolution data. Therefore, a three dimensional look-up-table $v_{0R}(M_a, \Omega, \theta)$ is calculated a priori from the cubic equation (197b), similar to van der Hooft and van Engelen (2004). Here, the equation (197b) is solved first in λ for numerical reasons. The aerodynamic torque M_a can then be calculated online from turbine data with (197a).

9.3.3 Linear Model

For the cyclic pitch feedforward controller (see Section 9.8), a model including the blade bending degree of freedom is needed. It is obtained from an azimuth dependent nonlinear aeroelastic model considering the rotor motion, first flapwise bending modes of each blade and the first tower fore-aft bending mode as depicted in Figure 117. The aeroelastic model is linearized, transformed with the Coleman-Transformation and decoupled, details see Schlipf et al. (2010b).

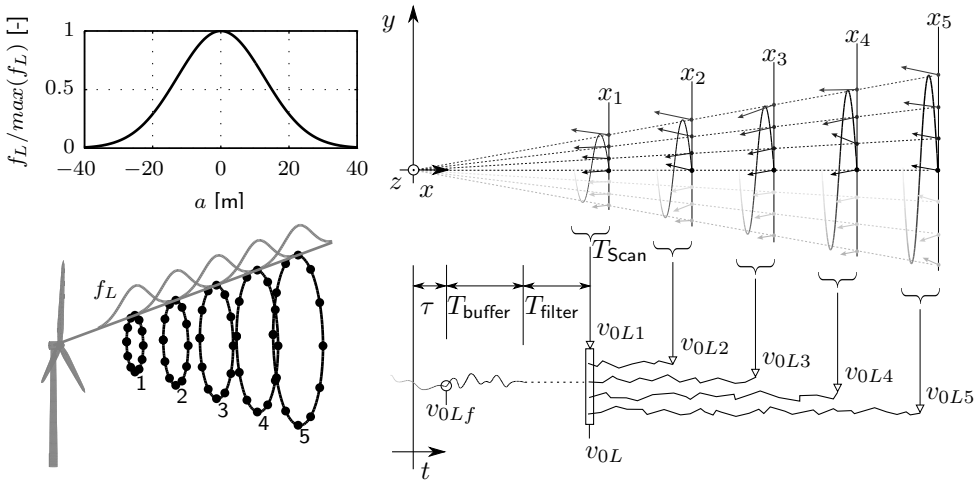

Figure 118: (left top) Normalized range weighing function $f_L(a)$ for a pulsed lidar system. (left bottom) Scope of circular scan (right) and the wind prediction.

9.4 Correlation of a Lidar System and a Wind Turbine

9.4.1 Simulated Lidar Measurements

Compared to (184) lidar measurements can be modeled more realistically for simulations by the following equation:

$$v_{los,i} = \int_{-\infty}^{\infty} \left(\frac{x_i}{f_i} u(a) + \frac{y_i}{f_i} v(a) + \frac{z_i}{f_i} w(a) \right) f_L(a) da. \tag{198}$$

The weighting function $f_L(a)$ at the distance a to the focus point depends on the used lidar technology (pulsed or continuous wave). Here, a Gaussian shape weighting function with full width at half maximum (FWHM) of $W = 30$ m is used, see Figure 118, following the considerations of Cariou (2011). 3D Wind fields generated e.g. with TurbSim (Jonkman and Buhl, 2007) over time t and the coordinates y and z can be scanned at a trajectory point $[t_i + T_{\text{Taylor},i}, y_i, z_i]$ by assuming Taylor's Hypothesis of Frozen Turbulence with

$$T_{\text{Taylor},i} = x_i / \bar{u}. \tag{199}$$

In this work, a pulsed system with a circular trajectory is used, which is performed within $T_{scan} = 2.4$ s with 12 focus points in 5 focus distances equally distributed between $0.5D$ and $1.5D$ with the rotor diameter $D = 126$ m, resulting in an update rate of 0.2 s, see Figure 118. This trajectory was realized by a real scanning lidar system installed on the nacelle of a 5 MW turbine (see Rettenmeier et al. (2010)). In the simulation, effects such as collision of the laser beam with the blades, volume measurement and mechanical constraints of the scanner from data of the experiment are considered to obtain realistic measurements.

9.4.2 Reconstruction of Rotor Effective Wind Speed

The wind characteristics are then reconstructed using (185): For each distance i the longitudinal wind component is averaged over the last trajectory for a rotor effective value and the obtained time series of the measurements v_{0Li} is time-shifted according to Taylor's frozen turbulence hypothesis, see Figure 118. The rotor effective wind speed $v_{0L}(t)$ is then calculated by

$$v_{0L}(t) = \frac{1}{5} \sum_{i=1}^{5} v_{0Li}(t - T_{\text{Taylor},i}). \tag{200}$$

This improves the short term estimation, because the measurements of further distances can be stored and used to obtain more information when reaching the nearest distance.

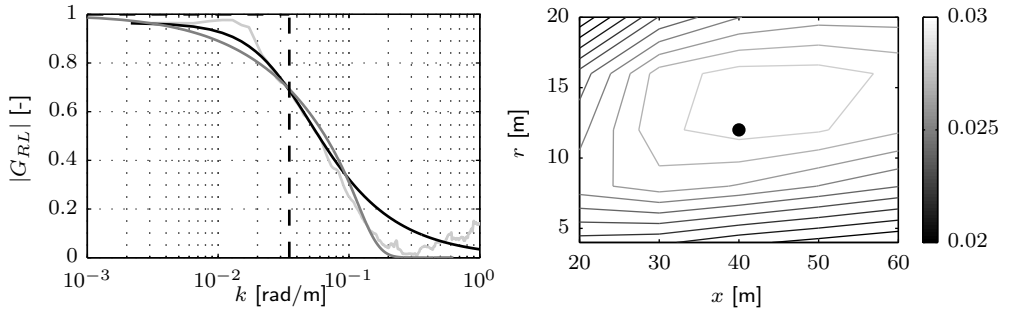

Figure 119: (left) Transfer function for a scanning lidar and a turbine: analytic (dark gray), measured (light gray), and fitted (black); maximum coherent wavenumber (dashed). (right) Optimization of the maximum coherent wavenumber.

9.4.3 Correlation

The correlation between the lidar estimate of the rotor effective wind speed v_{0L} and the rotor effective wind speed v_0 can be calculated by the transfer function

$$G_{RL} = \frac{S_{RL}}{S_{LL}} \tag{201}$$

and the squared coherence

$$\gamma^2_{RL} = \frac{|S_{RL}|^2}{S_{RR}S_{LL}} \tag{202}$$

using the auto spectrum S_{LL} from the lidar signal and S_{RR} from the rotor signal as well as the cross spectrum S_{RL} between the rotor and the lidar signal. With the definition of Bendat and Piersol (1971) cross and auto spectra can be calculated, omitting all scaling constants, by

$$\begin{aligned} S_{RR} &= \mathcal{F}\{v_0\}\mathcal{F}^*\{v_0\} \\ S_{RL} &= \mathcal{F}\{v_0\}\mathcal{F}^*\{v_{0L}\} \\ S_{LL} &= \mathcal{F}\{v_{0L}\}\mathcal{F}^*\{v_{0L}\}, \end{aligned} \tag{203}$$

where $\mathcal{F}\{\}$ and $\mathcal{F}^*\{\}$ are the Fourier transform and its complex conjugate, respectively. The same idea is used for the blade effective wind speed in Simley and Pao (2013).

For real time applications the spectra can be obtained from lidar measurements and turbine data using the estimator (197). The transfer function can be approximated by a standard low pass filter. Therefore, the maximum coherent wavenumber can be found with the cut-off frequency (-3 dB) of the corresponding filter (see Figure 119 in Schlipf and Cheng (2013)).

The correlation between a lidar system and a turbine can be calculated also analytically using analytic wind spectra, e.g. the Kaimal model. The measured wind can be considered as a sum of signals and due to the linearity of the Fourier transformation, the spectra can be calculated by a sum of auto and cross spectra, using (185), (198), and (200). In the full-analytical case, already the case of a staring lidar is very complicated. In the semi-analytical case, the rotor effective wind can be expressed by the mean of all n longitudinal wind components u_i hitting the rotor plane:

$$v_0 = \frac{1}{n}\sum_{i=1}^{n} u_i. \tag{204}$$

This model can then be used to design an optimal filter which is the crucial part of the controller described in the following sections. Another application is to optimize lidar systems (Schlipf et al., 2013a): Figure 119 shows how the maximum coherent wavenumber changes, if the focus distance x from a turbine with a rotor diameter of 40 m and the radius r of a scan with three measurements are varied. Furthermore, lidar measurements can be evaluated, whether the provided signal quality is sufficient for control, see e.g. Schlipf et al. (2012a); Scholbrock et al. (2013).

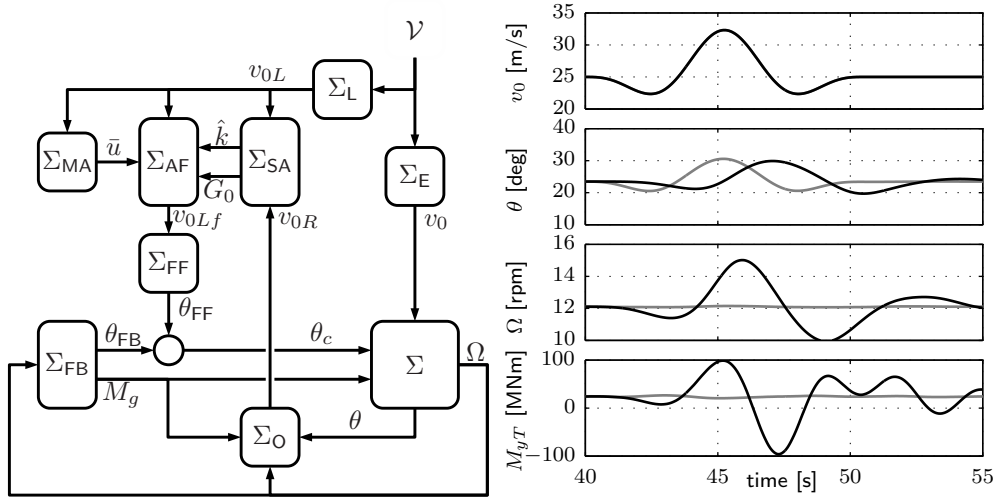

Figure 120: (left) Feedforward controller with adaptive filter. (right) Reaction to an EOG in case of perfect measurement using the 5 MW NREL turbine in FAST (Jonkman et al., 2009): Baseline controller only (black) and with additional feedforward (grey).

9.5 Lidar Assisted Collective Pitch Control

The lidar based collective pitch feedforward controller is the most promising approach for load reduction. In this section the controller and adaptive filter design will be presented and some results from the initial field testing.

9.5.1 Controller and Adaptive Filter Design

The collective pitch feedforward controller (see Figure 120) is based on the work in Schlipf et al. (2010a); Schlipf and Cheng (2013) and combines a baseline feedback controller with a feedforward update. The main control goal of the collective pitch feedback controller Σ_{FB} is to maintain the rated rotor speed Ω_{rated}. The system Σ is disturbed by a wind field $\mathcal{V}$, which can be measured by a lidar system Σ_{L} in front of the turbine before reaching the rotor. If the wind would not change on its way ($\Sigma_{\mathsf{E}} = 1$) and in the case of perfect measurement the measured wind speed v_{0L} and the rotor effective wind speed v_0 are equal. In this case and assuming a simple nonlinear wind turbine model (197), the effect of the wind speed on the rotor speed can perfectly compensated moving the collective pitch angle along the static pitch curve $\theta_{SS}(v_0)$ without any preview. If a more detailed model is used along with a pitch actuator, the proposed feedforward controller still can achieve almost perfect cancellation of an Extreme Operating Gust (EOG), see Figure 120. In this case, only a small preview time τ is necessary to overcome the pitch actuator dynamics.

In reality v_0 cannot be measured perfectly due to the limitation of the lidar system and Σ_{E} is quite complex to model. However, if the transfer function (201) from the measured wind speed to the rotor effective wind speed is known, it can be used to obtain a signal as close as possible to the rotor effective wind speed. Therefore, an adaptive filter is proposed along with a time buffer which can be fitted to the transfer function:

$$\Sigma_{\mathsf{AF}} = G_{\mathsf{filter}} e^{-T_{\mathsf{buffer}} s} \approx \Sigma_{\mathsf{E}}\ \Sigma_{\mathsf{M}}^{-1}. \tag{205}$$

The filter depends on the mean wind speed $\bar{u}$, which can be obtained with a moving average Σ_{MA}, and on the maximum coherent wavenumber $\hat{k}$ and the static gain G_0, which can be identified with a spectral analysis Σ_{SA} and the observer Σ_O from (188). The buffer time (see Figure 118) is necessary to apply the signal with the prediction time τ, considering the delay of the filter T_{filter} and the scan T_{scan}, assuming Taylor's Hypothesis:

$$T_{\mathsf{buffer}} = T_{\mathsf{Taylor}} - \frac{1}{2} T_{\mathsf{scan}} - T_{\mathsf{filter}} - \tau. \tag{206}$$

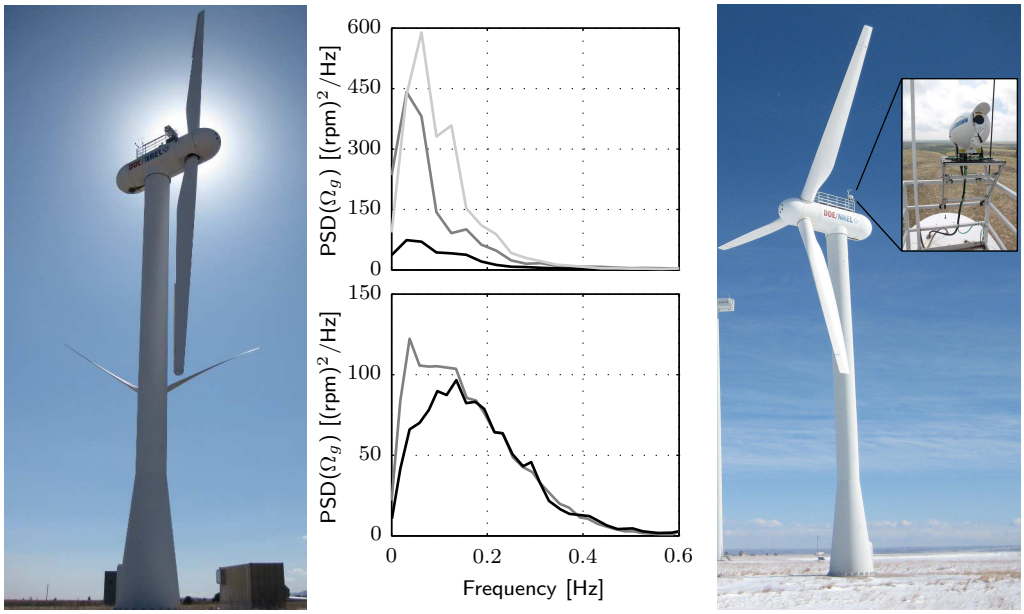

Figure 121: (left) The SWE-Scanner on the CART2. (middle) Spectra of the generator speed for the CART2 (top) and CART3 (bottom): FF off (dark gray), FF on with high (black) and low (light gray) correlation. (right) The OCS on the CART3.

9.5.2 Field Testing

The collective pitch controller has been successfully tested together with the National Renewable Energy Laboratory (NREL) in Boulder, Colorado in two different control campaigns. The scanning SWE-Lidar system was installed on the two-bladed CART2 and the OCS from Blue Scout Technologies on the three-bladed CART3. The main purpose of these campaigns was to provide a proof-of-concept of the feedforward controller. More details can be found in Schlipf et al. (2012a); Scholbrock et al. (2013).

In a first step the correlation between both turbines and the installed lidars was investigated, using the estimator (188). The maximum coherent wavenumber in the transfer function (201) was identified for the CART2 and the scanning lidar at $\hat{k} = 0.06$ rad/m and for the CART3 and the OCS at $\hat{k} = 0.03$ rad/m.

Then the adaptive filter and the feedforward controller was applied to each turbine. Here, a pitch rate update $\dot{\theta}_{\mathsf{FF}}$ instead of θ_{FF} was used:

$$\dot{\theta}_{\mathsf{FF}}(t) = \dot{v}_0(t+\tau)\frac{d\theta_{ss}}{dv_{0ss}}(v_0(t+\tau)) \tag{207}$$

Figure 121 shows the main result of the field testing, which is a reduction of the generator speed variations with the feedforward pitch rate update on, compared to the case with only the feedback controller. In the case of high correlation, the standard deviation of the rotor speed has been reduced by 30% for the CART2 and by 10% for the CART3. The difference is due to the lower correlation of the OCS on the CART3: The rotor speed is only reduced up to the frequency corresponding to the maximum coherent wavenumber.

However, in the case of low correlation, which was due to the impact with the met mast and guy wires, an increment of the generator speed variations can be seen, because of the wrong pitch action by the feedforward controller. This confirms, that it is possible to assisted wind turbine controllers with lidar measurements, but the signal has to be carefully filtered to have a beneficial effect.

Although load reductions have been detected as well, in next campaigns the feedback controller should be tuned: The benefit gained in rotor speed variation can be transformed in further load reduction by relaxing the feedback controller gains (Schlipf and Cheng, 2013).

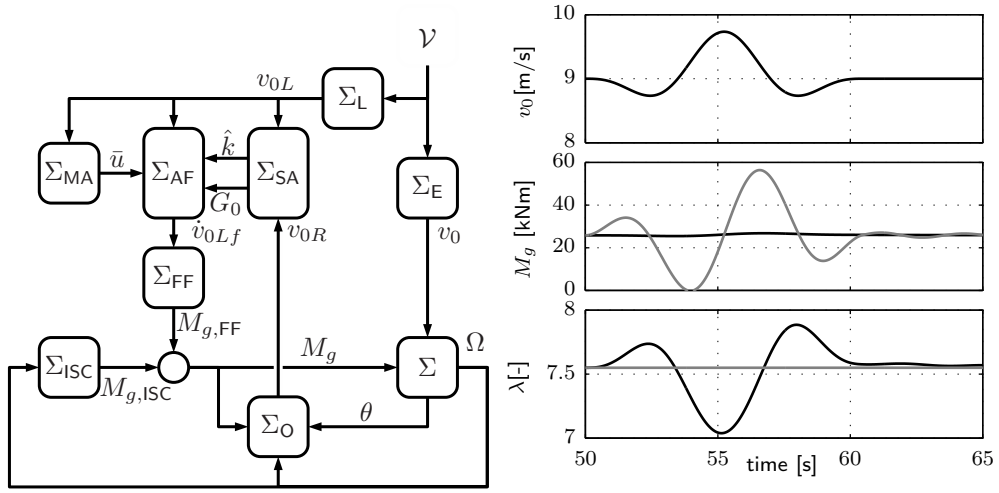

Figure 122: (left) Direct Speed Controller with adaptive filter. (right) Reaction to a gust in case of perfect measurement using the 5 MW NREL turbine in FAST (Jonkman et al., 2009): Baseline controller only (black) and with additional feedforward (grey).

9.6 Lidar Assisted Speed Control

The main purpose of variable speed control for wind turbines below rated wind speed is to maximize the electrical power extraction (Burton et al., 2001). Therefore, the turbine has to operate with the rotor blades held at the optimal angle of attack. This blade inflow angle is represented by λ (197c). The optimal tip speed ratio λ_{opt} can be found at the peak $\hat{c}_P$ of the power coefficient. The aerodynamic optimum can be achieved by tracking λ_{opt} via adjusting the generator torque M_g. This section depicts how tracking λ_{opt} can be done dynamically by using the knowledge of the incoming wind, more details see Schlipf et al. (2011, 2013b).

9.6.1 Controller Design

The baseline speed control (Burton et al., 2001) to maintain in steady state the maximum power coefficient $\hat{c}_P$ can be determined with the reduced nonlinear model (197) by:

$$M_{g,\mathsf{ISC}} = \underbrace{\frac{1}{2}\rho\pi R^5 \frac{\hat{c}_P}{\lambda_{opt}^3} i^3}_{k_{\mathsf{ISC}}} \Omega_g^2. \tag{208}$$

Equation (208) with constant k_{ISC} is known as the indirect speed control (ISC). Using the lidar technology, v_0 and thus λ become measurable, and therefore, the proposed controller is considered as direct speed control (DSC). The basic idea of the proposed DSC is to keep the ISC feedback law (208) and to find a feedforward update $M_{g,\mathsf{FF}}$ to compensate changes in the wind speed similar to the one used for collective pitch control, see Figure 120. With the derivative of the rotor effective wind speed $\dot{v}_0$ the DSC is:

$$M_{g,\mathsf{DSC}} = M_{g,\mathsf{ISC}} \underbrace{-iJ\frac{\lambda_{opt}}{R}\dot{v}_0}_{M_{g,\mathsf{FF}}}. \tag{209}$$

Higher order DSCs can be found (Schlipf et al., 2013b). Similar to the collective pitch feedforward controller, this controller in the nominal case perfectly maintains λ at its optimal value. This still holds, using a full aero-elastic model, assuming perfect measurement of v_0. But Figure 122 shows, that M_g has to be negative already with a small gust with 1 m/s amplitude due to the high inertia J, introducing high loads on the shaft.

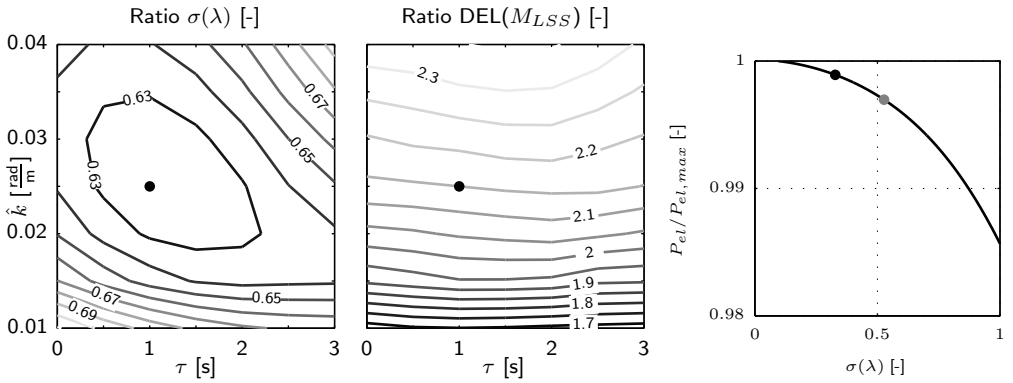

Figure 123: (left) Relative changes of the DSC in the standard deviation of λ and low-speed shaft loads compared to the ISC. Dots: optimal case. (right) Relative power extraction for the CART3. Dots: Field test results: ISC (gray) and DSC (black).

9.6.2 Simulation Using Real Data

The lidar raw data and the estimated v_{0R} obtained with (188) from the CART3 control campaign (see Figure 121) are used for simulations to test the DSC. The simulations are done with an aeroelastic model of the CART3 implemented in FAST (Jonkman and Buhl, 2005), disturbed by a hub height wind field of v_{0R}. The same adaptive filter (205) is used, see Figure 122. In this case the benefits over conventional simulations with lidar simulation and wind evolution models (Bossanyi, 2012) are that effects such as measurement errors and delays, real wind evolution, and site specific problems can be included into the simulations. If used along with the ISC controller, the simulated turbine's reaction will be close to the measured turbine data due to the fact that the used estimation of the rotor effective wind speed v_{0R} is an inverse process to the simulation. If used along with the DSC controller, it can be estimated in a realistic way, which effect the DSC would have produced in this specific situation. Furthermore, the DSC can be tuned to the real data.

A set of simulations with different $\hat{k}$ and τ are done. Figure 123 shows the changes from the DSC to the ISC in the standard deviation of λ and damage equivalent loads (DEL) on the low-speed shaft. The optimal values for $\hat{k} = 0.025$ rad/m and $\tau = 1$ s from this brute force optimization (minimizing $\sigma(\lambda)$) are close to the value from Section 9.5. This confirms, that it is important to filter the data according to this specific correlation.

Here, the standard deviation $\sigma(\lambda)$ can be reduced from 0.527 to 0.328, resulting in a power production increase of 0.3%, which is close to the theoretical value of 0.2% from Figure 123. The loads on the shaft are approximately doubled. This proofs, that only marginal benefit can be gained by tracking the optimal tip speed ration, which does not justify the usuage due to the higher loads on the shaft.

9.6.3 Discussion

The fluctuation of the tip speed ratio can be used as a measure for the potential of energy optimization. Assuming the distribution of the tip speed ratio $\varphi_{\lambda_{opt};\sigma}$ to be Gaussian with mean λ_{opt} and a standard deviation $\sigma(\lambda)$, then the generated power can be estimated by

$$P_{el}(\sigma(\lambda)) = P_{el,max} \int_{-\infty}^{\infty} \varphi_{\lambda_{opt};\sigma(\lambda)} c_P(\lambda) d\lambda. \tag{210}$$

The collected data from the CART3 field testing justify a Gaussian distribution (Schlipf et al., 2013b). In Figure 123 this potential is quantified for the CART3.

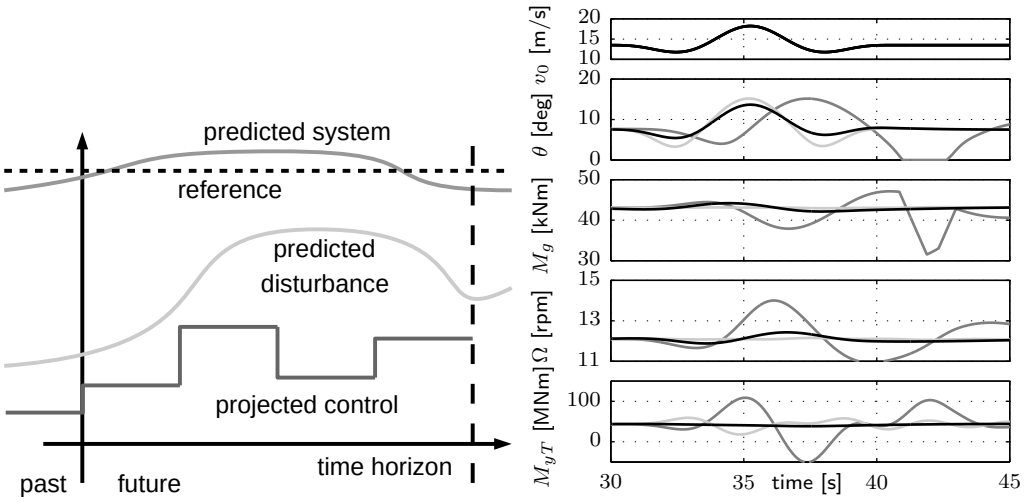

Figure 124: (left) Principle of NMPC. (rigth) Reaction to an EOG in case of perfect measurement using the 5 MW NREL turbine in FAST (Jonkman et al., 2009): Baseline controller only (dark gray), baseline with feedforward (light grey) and NMPC (black).

9.7 Nonlinear Model Predictive Control

Model predictive control (MPC) is an advanced control tool, which predicts the future behavior of the system using an internal model and the current measurements. With this information the control actions necessary to regulate the plant are computed by solving an optimal control problem over a given time horizon. Part of the solution trajectory for the control inputs are transfered to the system, new measurements are gathered and the optimal control problem is solved again. The feedforward controller presented in the previous sections are updates to existing pitch and torque feedback controllers. In contrast the MPC is a control strategy which in the presented case controls pitch angle and generator torque independently from the common feedback controllers. This provides the possibility for further improvements, but also makes real applications more complex. Here, the basic principle and simulation results of a nonlinear model predictive control (NMPC) are presented. More details can be found in Schlipf et al. (2012b,d).

9.7.1 Controller Design

There are several advantages of MPC in general. One is that it can handle multi-variable and non-quadratic (different number of inputs and outputs) control tasks naturally: additional control inputs or outputs will merely increase the number of optimization variables. Another advantage is that it considers actuator and system constraints during solving the optimal control problem. Furthermore, it provides a framework for incorporating a disturbance preview dynamically and tuning of MPC controllers is done intuitively by changing weights of a definable objective function. However, the main advantage of MPC is that it is in a mathematically sense an optimal controller. Solving the optimal control problem is not an easy task and several methods exist. Independent of the used method, the basic principle of model predictive control is illustrated in Figure 124 using piecewise constant parametrization: Future control action is planned to fulfill the control goal, e.g. reference signal tracking, considering a predicted disturbance. The considered optimal wind turbine control problem can be described by the following problem: The objective is to find the optimal control trajectory which minimizes the cost function, which is defined as the integral over the time horizon of the objective function from the actual time to the final time, with the reduced nonlinear model (192) and the set of constraints. The crux of designing the NMPC is to translate the verbal formulation of the control goal to a mathematical formulation. In wind energy the overall goal of development can be stated very roughly as “minimizing energy production cost”. In

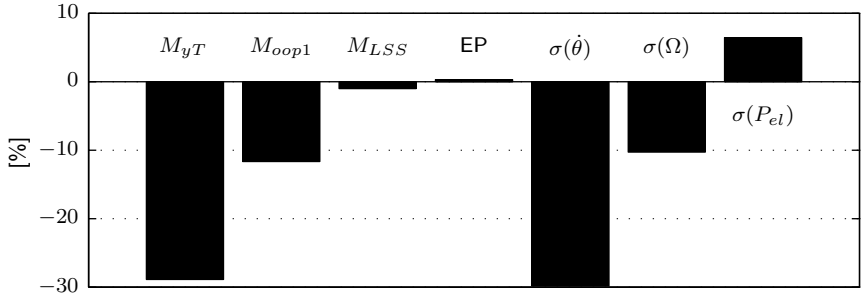

Figure 125: Overall improvement for the NMPC with respect to the baseline: Lifetime weighted DEL for tower base fore-aft bending moment M_{yT}, out-of-plane blade root bending moment of blade 1 M_{oop1} and low-speed shaft torque M_{LSS}, lifetime energy production, lifetime weighted standard deviation of pitch rate, rotor speed and electrical power.

classic wind turbine control (Burton et al., 2001) this is in general done by tracking optimal tip speed ratio below a certain wind speed defined as rated wind speed and by limiting rotor speed and power above the rated wind speed. The used objective function and constraints can be found in Schlipf et al. (2012b).

The optimal control problem is converted by the Direct Multiple Shooting method (Findeisen, 2005) into a nonlinear program. The control inputs are discretized in piecewise constant stages and the ODEs of the model are solved numerically on each interval. The optimization is performed over the set of initial values and the control outputs. Additional constraints are applied to ensure that the states at the end of each stage coincide with the initial conditions of the subsequent stage.

The nonlinear program can be solved iteratively with Sequential Quadratic Programming (SQP). The separation of the optimization problem into multiple stages results in a faster solution. Here Omuses (Franke, 1998) is used, a front-end to the large-scale SQP-type nonlinear optimization solver HQP.

9.7.2 Simulation Results

In a first step the different control strategies are compared with their reaction to gusts. For this purpose, hub-height time series are created with extreme operation gusts at $v_{rated} + 2$ m/s $= 13.2$ m/s. At first the simulations are run with the reduced nonlinear model such that the internal model and the simulation model are identical. Furthermore, the wind speed is directly fed into the NMPC assuming perfect measurements and the tower states are assumed to be measurable. This is done to make results more apparent and to show the effect of different optimization goals: The NMPC tries to reduce rotor speed variation and the tower movement. Figure 124 compares the pitch angle, generator torque, rotor speed, and tower base fore-aft bending moment for the baseline controller, the feedforward controller of Section 9.5 and the NMPC. The NMPC and the feedforward controller are able to minimize the rotor speed deviation. The feedforward controller only uses the pitch angle to achieve this goal. The NMPC additionally uses the generator torque to achieve the minimization of the tower movement and the variation of the rotor speed due to its competence to incorporate multivariable control.

In a second step various simulations with a set of turbulent TurbSim wind fields are conducted, featuring A-type turbulence intensity according to IEC 61400-1 and a Rayleigh distribution with $C = 12$ m/s, to estimate the benefit for fatigue load reduction. The adaptive filter (205) and a nonlinear estimator (Schlipf et al., 2012b) are used.

Figure 125 summarizes the results for all 33 simulations. Even if the NMPC controller is computationally more complex, the framework provides a high performing benchmark for development and comparison of less computationally-complex controllers.

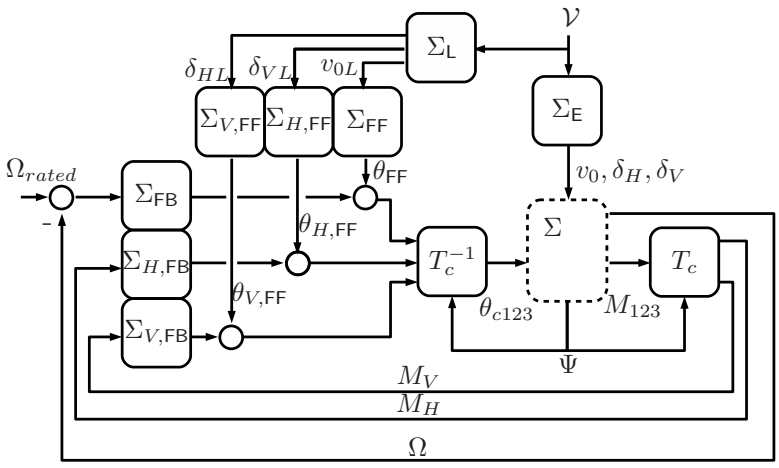

Figure 126: Cyclic pitch feedforward control: The feedforward controllers try to compensate the effects of the wind field $\mathcal{V}$ on the rotor speed Ω and the horizontal and vertical blade root bending moments, M_H and M_V.

9.8 Lidar Assisted Cyclic Pitch Control

The block diagram in Figure 126 illustrates the used feedforward control schema for the cyclic pitch control problem. More details can be found in Dunne et al. (2012), Schlipf et al. (2010b) and Laks et al. (2011).

The collective pitch controller is extended by two additional control loops: The flapwise blade root bending moments of the three blades M_{123} are transformed by the Coleman transformation T_c into a yaw and tilt moment M_H and M_V. These signals are fed back into two additional feedback controllers $\Sigma_{H,\mathsf{FB}}$ and $\Sigma_{V,\mathsf{FB}}$. Here, standard PI controllers are used following those of Bossanyi et al. (2012). The horizontal and vertical blade root bending moment M_H and M_V are mainly disturbed by the horizontal and vertical shear δ_H and δ_V. The shears can also be estimated by a lidar system (see Section 9.2) and can be used to calculate the feedforward updates $\theta_{H,\mathsf{FF}}$ and $\theta_{H,\mathsf{FF}}$ for the horizontal and vertical control loop. Static functions are proposed, which can be obtained from simulations or from modeling:

$$\theta_{H,\mathsf{FF}} = g_H \delta_{HL} \tag{211}$$

$$\theta_{V,\mathsf{FF}} = g_V \delta_{VL}$$

Furthermore, the same filter (205) is used to avoid wrong pitch action. Also the time tracking issue is solved similar to the collective pitch feedforward controller: The feedforward update is added to the feedback with the prediction time τ before the shears reach the turbine.

To demonstrate the benefit of lidar assisted cyclic pitch control, a collective pitch feedback only controller is compared to a cyclic pitch feedback only controller and a combined collective and cyclic feedback and feedforward controller. A wind field with mean wind speed $\bar{u} = 16$ m/s and a turbulence intensity of 18% is used. Figure 127 shows the power spectral densities of pitch rate and out-of-plane blade root bending moment of blade 1. Both individual pitch controllers decrease variation of the blade root bending moment especially at the $1P$ frequency, but only the feedforward controller can reduce the loads around 0.1 Hz due to the collective feedforward part. Further investigations have to be done to investigate, whether similar load reduction can be obtained without the cyclic feedforward part. A validation of the lidar reconstructed rotor effective wind characteristics can be achieved by comparing to those estimated from turbine data. Figure 128 compares the shears obtained from model (186) with shears obtained by a simple estimation from blade root bending moment, showing as expected a better correlation for δ_V than for δ_H. Further investigations have to be done in addition to investigate, if the correlation between the lidar measurement and the turbine reaction regarding the shears is sufficient to use it for feedforward control.

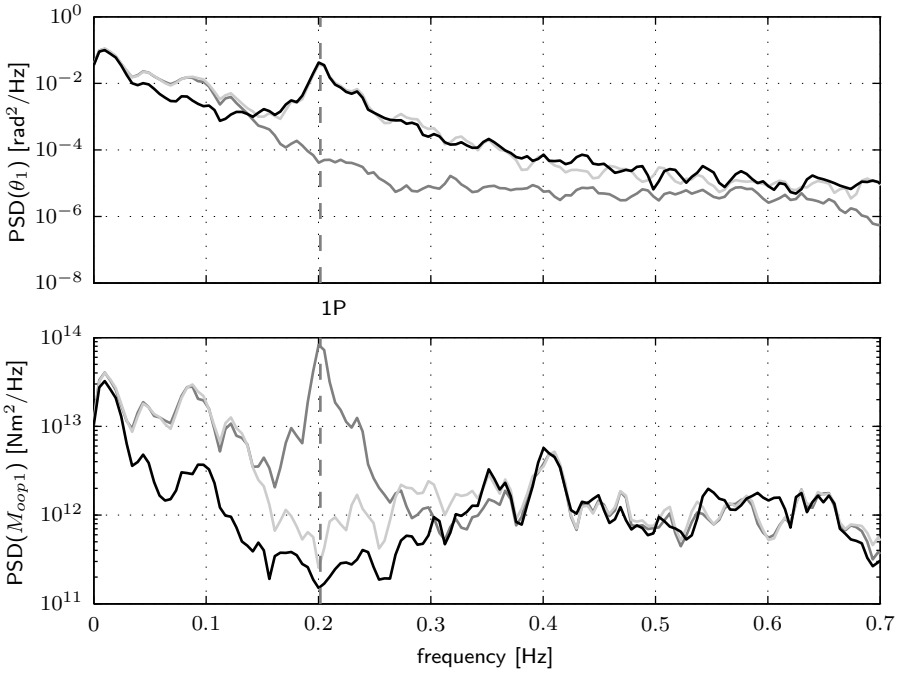

Figure 127: Power spectral density of pitch rate and out-of-plane blade root bending moment of blade 1: Collective pitch feedback (dark gray), cyclic pitch feedback (light gray) and combined collective and cyclic feedback and feedforward (black). The cyclic pitch controller decrease the spectra around the 1P frequency at the expense of higher pitch action in this frequency section.

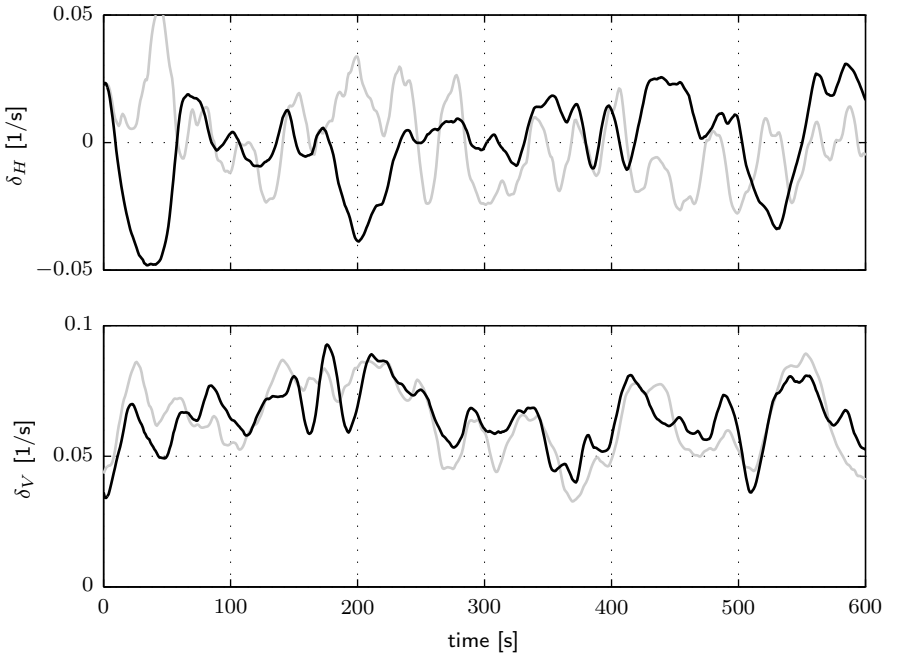

Figure 128: Estimated (1 min average) shears using lidar (black) and turbine data (gray). The correlation of the vertical shear (bottom) is higher than the correlation of the horizontal shear (top).

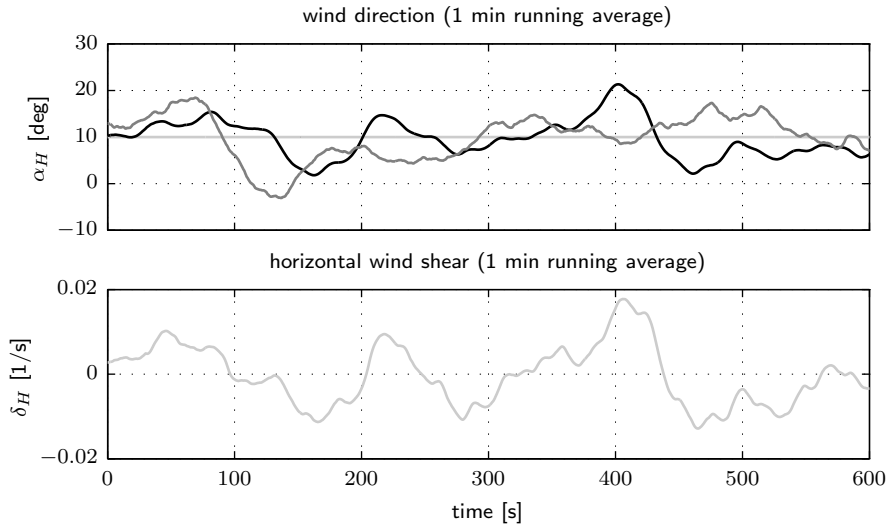

Figure 129: Misalignment and horizontal shear. From a wind field (light gray), lidar estimation (black) and sonic anemometer simulation (dark gray).

9.9 Lidar Assisted Yaw Control

Due to the large moment of inertia of the rotor, the nacelle is aligned with the wind with slow rates and only, if the misalignment exceeds a certain value (Hau, 2008). The demand signal is normally calculated from a nacelle mounted wind vane or sonic anemometer. These sensors are heavily disturbed for an operating turbine and are measuring at only one single point. A nacelle mounted lidar system avoids these disadvantages, being able to measure the undisturbed inflow over the entire rotor area. The first part of this section shows the capability and the problems of a simulated lidar system. In the second part data is analyzed and finally in the third part the improvements in energy yield by lidar assisted yaw control are discussed theoretically. More details can be found in Schlipf et al. (2011).

9.9.1 Simulation Using Generic Wind

The scope of the presented simulation study is to test if the methods presented in Section 9.2 are robust and can be applied to turbulent wind fields. This is not obvious, because the simulation model of the wind (here IEC Kaimal) and of the lidar (198) are more complex than the wind (189) and lidar (184) model used in the reconstruction. Similar work has been presented (Kragh et al., 2011), using an empiric reconstruction method and Mann turbulence.

The 33 Class A wind fields from Section 9.6 are generated with a horizontal mean flow angle of $\alpha_H = 10$ deg. The 10 min-wind fields are scanned again with the mentioned lidar simulator, imitating the SWE-lidar system (Rettenmeier et al., 2010) using a Lissajous-like trajectory. The misalignment detected by the lidar α_{HL} is estimated with the model (189) using those focus points from the last n points, where no impact with the turbine blades is simulated. Due to the positioning on top of the nacelle, similar to the one used in the experiment, this usually results in a loss of $\approx 30\%$. The resulting α_{HL} signal is very oscillating and for better illustration a 1 min running average is used in Figure 129. Due to the effects described in Section 9.2 the misalignment signal estimated with the lidar is disturbed by the horizontal shear. For comparison, the misalignment signal of a point measurement is plotted, which could be obtained from an undisturbed sonic anemometer on hub height.

For all 33 simulations the error of the misalignment estimation in the 10 min mean is below 1 deg due to the fact that the mean of the effective horizontal shear for the wind field is close to zero. The results of this simulation study show that with the proposed method of wind reconstruction it is possible for a simulated lidar to estimate the misalignment of a turbine in the scale of 10 min similar to the simulated undisturbed sonic anemometer.

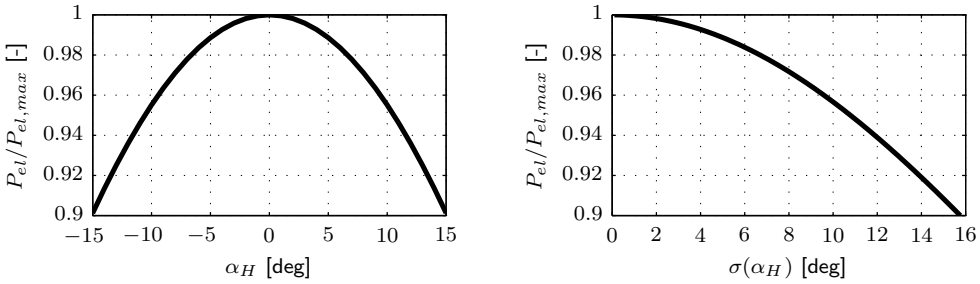

Figure 130: Power loss due to static (left) and dynamic (right) misalignment.

9.9.2 Simulation Using Real Data

From the simulation study above it is hard to estimate the improvement of lidar assisted yaw control compared to the standard control. Therefore, a simulation study can be done using data from a real experiment. The absolute yaw direction signal is superposed with the relative, 10 min averaged misalignment signals from the nacelle mounted lidar and sonic anemometer. With this method it can be simulated, how the turbine would have been yawed for both instruments, if the same yaw control strategy is applied. Finally, the resulting yaw misalignment for both instruments can be calculated by comparing the simulated turbine positions with the lidar wind direction, assuming the lidar is able to perfectly estimate the averaged misalignment. Due to the average time and the threshold in the control strategy, the difference in the fluctuation of both signals is relatively low.

9.9.3 Discussion

Both studies above show, the yaw misalignment can be divided in a static and a dynamic subproblem. In reality there will be a mixture of both, but this perception is helpful to rate the benefits which can be achieved by using a lidar system for yaw control. If there is a static misalignment $\bar{\alpha}_H$, the loss in power can be modeled as (Burton et al., 2001):

$$P_{el}(\bar{\alpha}_H) = P_{el,max} \cos^3(\bar{\alpha}_H). \tag{212}$$

Figure 130, shows e.g. that $\approx 10\%$ of power is lost, if the turbine is misaligned by ≈ 15 deg to one side. This value can be considered as a lower bound, because a misalignment in full load operation will not have an effect on the power. A static misalignment can be solved by better calibration of the standard nacelle anemometer and does not need a constant use of a lidar system. In the case of the investigated data the detected static misalignment of 0.7 deg only would cause a power loss of 0.02%. A constant use of a nacelle mounted lidar system is justified, if the fluctuation of yaw misalignment can be reduced. Similar to the discussion in Section 9.6.3 the misalignment can be assumed to be Gaussian distributed with zero mean and a standard deviation $\sigma(\alpha_H)$. Then the loss in power can be modeled by:

$$P_{el}(\sigma(\alpha_H)) = P_{el,max} \int_{-\infty}^{\infty} \varphi_{0;\sigma(\alpha_H)} \cos^3(\alpha_H) d\alpha_H. \tag{213}$$

The loss in power due to the dynamic misalignment is plotted in Figure 130 and again is only applicable to partial load operation. The reduction of $\sigma(\alpha_H)$ and an improvement of the power output is limited to the control strategy: a reduction to 0 deg would require immediate yawing of the rotor which is neither feasible nor reasonable due to the induced loads. In the presented investigation a reduction from 6.4 deg to 4.1 deg yield to an improvement from $99.3\% - 98.2\% = 1.1\%$ using (213). This low value despite of assumed perfect reconstruction of the alignment by the lidar system gives an estimation of improvement which can be expected.

9.10 Conclusion and Outlook

Lidar systems are able to provide preview information of wind disturbances at various distances in front of wind turbines. This technology paves the way for new control concepts, helping to compensate changes in the inflowing wind field. The complexity of the wind field, the limitation due to the measurement principle and the combined aero-elastic character of wind turbines makes this an interdisciplinary and challenging task. This field of research has increased significantly in recent years and several controllers have been proposed for load reduction or increasing the energy yield.

In this work a method is presented to reconstruct wind characteristics based on lidar measurements and shortcomings are shown. This method is used in various approaches to increase the energy production and to reduce loads of wind turbines: Collective pitch feedforward control and direct speed control uses the knowledge of the incoming wind speed to calculate a control update to existing feedback controllers. Collective pitch feedforward control is a promising strategy to reduce extreme and fatigue loads and has been successfully tested. Filtering the lidar signal is an important issues, because not all turbulences can be measured. The filter can be designed based on the correlation between the lidar measurement and the reaction of the wind turbine. With the direct speed control only marginal benefit can be gained. This is due to the fact that the standard variable speed control is already close to the aerodynamic optimum. The approach of the Nonlinear Model Predictive Control differs from the feedforward approaches: the future behavior of a wind turbine is optimized by solving an optimal control problem repetitively using the wind speed preview adjusting simultaneously the pitch angle and the generator torque. Therefore, loads on tower, blades and shaft can be further reduced especially for wind conditions near rated wind speed. Further load reduction of the blades can be gained with cyclic pitch feedforward control, extending the feedforward approach to reduce also tilt and yaw moments of the rotor. Another approach uses the wind direction estimation by a lidar system for yaw control. Here, an increase of energy production by a couple of percent can be expected, depending on the control strategy and the inhomogeneity of the wind.

Acknowledgement

This research is funded by the German Federal Ministry for the Environment, Nature Conservation and Nuclear Safety (BMU) in the framework of the German joint research project "LIDAR II - Development of nacelle-based LIDAR technology for performance measurement and control of wind turbines". Thanks all the people getting the lidar systems and the different measurement campaigns working, special thanks to Jan Anger, Oliver Bischoff, Florian Haizmann, Martin Hofsäß, Andreas Rettenmeier and Ines Würth of the SWE Lidar group, Paul Fleming, Andrew Scholbrock and Alan Wright from NREL, my supervisors Po Wen Cheng, Martin Kühn and Lucy Pao and my students Valeria Basterra, Patrick Grau, Stefan Kapp, Timo Maul and Davide Trabucchi. Thanks to Björn Siegmeier from AREVA Wind GmbH for his help and the access to the turbine measurement data.

Notation

DEL	Damage Equivalent Loads
EOG	extreme operating gust
NMPC	Nonlinear Model Predictive Control
PI	proportional-integral (controller)
a	distance to focus point
A	constant variables for least squares method
c_P,c_T	power and thrust coefficient
d	system disturbance
D	rotor diameter
f_i	focus length of measurement point i

f_L	weighting function
G_{RL}	transfer function from the lidar estimate to the rotor effective wind speed
i	gearbox ratio
J	sum of the moments of inertia about the rotation axis of the rotor hub
$\hat{k}$	maximum coherent wave number
m	known variables for least squares method
m_{Te}, c_{Te}, k_{Te}	the tower equivalent modal mass, structural damping and bending stiffness
M_g	generator torque
M_a, F_a	aerodynamic torque and aerodynamic
M_{yT}	tower fore-aft bending moment
M_{LSS}	low speed shaft torque
M_{oop1}	out-of-plane bending moment
n	number of measurements
R	rotor radius
S_{RL}	cross spectrum between the lidar estimate to the rotor effective wind speed
S_{LL}	auto spectrum of the lidar estimate of the rotor effective wind speed
S_{RR}	auto spectrum of the rotor effective wind speed
s	unknown variables for least squares method
$T_{\text{Taylor},i}$	time delay based on Taylor's Hypothesis of Frozen Turbulence from point i
T_{scan}	time to finish a full scan
T_{buffer}	time to buffer data before applying the feedforward command
T_{filter}	time delay due to filtering
u	system input
u_i, v_i, w_i	local wind components in measurement point i
$\bar{u}$	mean wind speed
v_0	rotor effective wind speed
v_{0L}	estimate of rotor effective wind speed from lidar data
v_{0Lf}	filtered estimate of rotor effective wind speed from lidar data
v_{0R}	estimate of rotor effective wind speed from turbine data
$v_{los,i}$	line-of-sight wind speed in measurement point i
v_{rel}	relative wind speed
x	system states
x_i, y_i, z_i	coordinates of measurement point i in lidar coordinate system
x_{Wi}, y_{Wi}, z_{Wi}	coordinates of measurement point i in wind coordinate system
x_T	tower top displacement
y	system output
α_H, α_V	horizontal and vertical inflow angle
γ^2_{RL}	coherence between the lidar estimate to the rotor effective wind speed
δ_H, δ_V	horizontal and vertical shear
λ	tip speed ratio
ξ, ω	damping factor and undamped natural frequency of the pitch actuator
ρ	air density
τ	prediction time of a signal
$\varphi_{\bar{x};\sigma(x)}$	Gaussian probability density function depending on mean $\bar{x}$ and standard deviation $\sigma(x)$
θ, θ_c	collective pitch angle and collective pitch angle demand
θ_{FF}	feedforward pitch angle
Ω, Ω_g	rotor and generator speed
$\mathcal{V}$	wind field

References

D. Schlipf, T. Fischer, C. E. Carcangiu, M. Rossetti, and E. Bossanyi, "Load analysis of look-ahead collective pitch control using LiDAR," in *Proceedings of the German Wind Energy Conference DEWEK*, Bremen, Germany, 2010.

D. Schlipf, P. Fleming, F. Haizmann, A. Scholbrock, M. Hofsäß, A. Wright, and P. W. Cheng, "Field testing of feedforward collective pitch control on the CART2 using a nacelle-based lidar scanner," in *Proceedings of The Science of Making Torque from Wind*, Oldenburg, Germany, 2012.

A. Scholbrock, P. Fleming, L. Fingersh, A. Wright, D. Schlipf, F. Haizmann, and F. Belen, "Field testing LIDAR based feed-forward controls on the NREL controls advanced research turbine," in *51th AIAA Aerospace Sciences Meeting Including the New Horizons Forum and Aerospace Exposition*, Dallas, USA, 2013.

D. Schlipf, S. Kapp, J. Anger, O. Bischoff, M. Hofsäß, A. Rettenmeier, U. Smolka, and M. Kühn, "Prospects of optimization of energy production by LiDAR assisted control of wind turbines," in *Proceedings of the EWEA Annual event*, Brussels, Belgium, 2011.

D. Schlipf, D. J. Schlipf, and M. Kühn, "Nonlinear model predictive control of wind turbines using LIDAR," *Wind Energy*, 2012.

F. Dunne, D. Schlipf, L. Y. Pao, A. D. Wright, B. Jonkman, N. Kelley, and E. Simley, "Comparison of two independent lidar-based pitch control designs," in *Proc. 50th AIAA Aerospace Sciences Meeting Including the New Horizons Forum and Aerospace Exposition*, 2012.

D. Schlipf, A. Rettenmeier, M. Hofsäß, M. Courtney, and P. W. Cheng, "Model based wind vector field reconstruction from lidar data," in *Proceedings of the German Wind Energy Conference DEWEK*, Bremen, Germany, 2012.

J. Jonkman and M. L. Buhl, "FAST user's guide," NREL, Tech. Rep. NREL/EL-500-38230, August 2005.

B. J. Jonkman and M. L. Buhl, "TurbSim user's guide," NREL, Tech. Rep. NREL/TP-500-41136, April 2007.

C. L. Bottasso, A. Croce, B. Savini, W. Sirchi, and L. Trainelli, "Aero-servo-elastic modelling and control of wind turbines using finite-element multibody procedures," *Multibody System Dynamics*, vol. 16, pp. 291–308, 2006.

J. Jonkman, S. Butterfield, W. Musial, and G. Scott, "Definition of a 5-MW reference wind turbine for offshore system development," *Technical Report NREL/TP-500-38060*, 2009.

E. van der Hooft and T. G. van Engelen, "Estimated wind speed feed forward control for wind turbine operation optimization," *European Wind Energy Conference, London*, vol. 1, p. 9, 2004.

D. Schlipf, S. Schuler, P. Grau, F. Allgöwer, and M. Kühn, "Look-ahead cylcic pitch control using LiDAR," in *Proceedings of The Science of making Torque from Wind*, Heraklion, Greece, 2010.

J. P. Cariou, "Pulsed lidars," in *Remote Sensing for Wind Energy. Risøreport Risø-I-3184(EN)*. Roskilde, Denmark: A. Peña and C. B. Hasager, June 2011, pp. 65–81, Risø-DTU.

A. Rettenmeier, O. Bischoff, M. Hofsäß, D. Schlipf, J. J. Trujillo, and M. Kühn, "Wind field analysis using a nacelle-based lidar system," in *Presentation at the European Wind Energy Conference*, Warsaw, Poland, 2010.

J. S. Bendat and A. G. Piersol, *Random data; analysis and measurement procedures*. New York, USA: John Wiley & Sons, 1971.

E. Simley and L. Pao, "Correlation between rotating LIDAR measurements and blade effective wind speed," in *51th AIAA Aerospace Sciences Meeting Including the New Horizons Forum and Aerospace Exposition*, Dallas, USA, 2013.

D. Schlipf and P. W. Cheng, "Adaptive Vorsteuerung für Windenergieanlagen," *at - Automatisierungstechnik*, vol. 61, pp. 329–338, 2013.

D. Schlipf, J. Mann, and P. W. Cheng, "Model of the correlation between lidar systems and wind turbines for lidar assisted control," *submitted to Journal of Atmospheric and Oceanic Technology*, 2013.

T. Burton, N. Jenkins, D. Sharpe, and E. Bossanyi, *Wind Energy Handbook*. New York, USA: John Wiley & Sons, 2001.

D. Schlipf, P. Fleming, S. Kapp, A. Scholbrock, F. Haizmann, F. Belen, A. Wright, and P. W. Cheng, "Direct speed control using lidar and turbine data," in *Proceedings of the American Control Conference*, Washington, USA, 2013.

E. Bossanyi, "Un-freezing the turbulence: improved wind field modeling for investigating lidar-assisted wind turbine control," in *Proceedings of the EWEA Annual event*, Copenhagen, Denmark, 2012.

D. Schlipf, L. Y. Pao, and P. W. Cheng, "Comparison of feedforward and model predictive control of wind turbines using LIDAR," in *Proceedings of the Conference on Decision and Control*, Maui, USA, 2012.

R. Findeisen, "Nonlinear model predictive control: A sampled-data feedback perspective," Ph.D. dissertation, Universität Stuttgart, 2005.

R. Franke, "Omuses - a tool for the optimization of multistage systems and HQP a solver for sparse nonlinear optimization," TU Ilmenau, Tech. Rep., 1998.

J. Laks, L. Y. Pao, E. Simley, A. Wright, N. Kelley, and B. Jonkman, "Model predictive control using preview measurements from LIDAR," in *Proceedings of the 49th AIAA Aerospace Sciences Meeting Including the New Horizons Forum and Aerospace Exposition*, Orlando, USA, 2011.

E. Bossanyi, B. Savini, M. Iribas, M. Hau, B. Fischer, D. Schlipf, T. van Engelen, M. Rossetti, and C. E. Carcangiu, "Advanced controller research for multi-MW wind turbines in the UpWind project," *Wind Energy*, vol. 15, no. 1, pp. 119–145, 2012.

E. Hau, *Windkraftanlagen*, 4th ed. Springer, 2008.

A. Kragh, M. Hansen, and T. Mikkelsen, "Improving yaw alignment using spinner based LIDAR," in *Proc. 49th AIAA Aerospace Sciences Meeting Including the New Horizons Forum and Aerospace Exposition*, 2011.